



Growth Technique–Induced Highly C-Axis-Oriented ZnO: Mn, ZnO: Fe and ZnO: Co Thin Films: A Comparison of Nanostructure, Surface Morphology, Optical Band Gap, and Room Temperature Ferromagnetism

Sultan Goktas¹ · Ahmet Tumbul² · Abdullah Goktas³

Received: 26 May 2023 / Accepted: 18 September 2023 / Published online: 12 October 2023
© The Author(s), under exclusive licence to Springer Science+Business Media, LLC, part of Springer Nature 2023

Abstract

In this study, highly c-axis-oriented ZnO:TM (TM = Co, Fe, and Mn) thin films doped with different doping levels ($x = 0–10$ at%) of TM were grown by chemical (sol-gel) and physical (magnetron sputtering) film deposition methods. These films were scrutinized by XRD, AFM, FESEM, EDX, XPS, Uv-Vis spectrophotometer, and VSM magnetometer. All the films have a powerful preferential c-axis orientation with a hexagonal polycrystalline structure. Comparatively, the stronger c-axis orientation and higher crystalline quality were observed for the chemically fabricated films than those physically derived. The chemically derived films had relatively higher roughness and it was decreased with increasing TM doping concentration. Compared to the ZnO, an increment in the crystallinity of chemically derived films was observed with an enhanced TM doping ratio, whereas a decrement in physically derived films was observed. The existence of Zn, Mn, Co, Fe, and O atoms and Zn^{2+} , Co^{2+} , Mn^{2+} , and Fe^{2+} ions were determined. Optical analysis revealed that the transmittance of chemically derived ZnO:TM thin films was relatively higher than physically produced, and the optical band gap of the films produced by both techniques was in good agreement with each other except for the ZMO. Magnetic measurements showed a clear room temperature ferromagnetic behavior for the ZnO:Mn and ZnO:Fe films. In contrast, paramagnetic behavior was observed for the chemically and physically produced ZnO:Co films. Among all films, the highest ferromagnetic response was obtained for the ZnO:Fe films due to their high crystallinity and purity. These outcomes reflect the produced films have great potential to be promising materials for optoelectronic and spintronic applications.

Keywords ZnO: dopants (Mn, Fe, and Co) · Optical transmittance · Band gap energy · Chemically derived films · Physically derived films · Room temperature ferromagnetism

1 Introduction

Nanostructured ZnO is the most important semiconductor, having many applications because of its technological substance and interesting characteristics such as relatively high chemical stability, non-toxic, environmentally friendly, biocompatible nature, tunable structural, optical, electrical, and

magnetic properties via doping [1, 2]. ZnO-nanostructured semiconductors have wide potential applications, like light-emitting diodes, photovoltaic, photocatalysis, lasers, biological labeling, catalysis, and sensors [3–5]. This is owing to its wide band gap, relatively good thermal stability, and large exciton binding energy as well as the quantum confinement effect and higher surface area-to-volume ratio in its nano-sized structures.

In potential applications, it is very crucial to have relatively high crystalline quality/optical quality and low surface roughness to get high performance. For example, Rana et al. [9] have shown that the optical transparency and the film quality of the ZnO layer need to be high enough for the transparent photovoltaic. Luo et al. [10] have reported the importance of the ZnO morphology and its intrinsic properties, which could be easily tuned by the chemical solution process for the perovskites solar cell. Rather than all, the

✉ Abdullah Goktas
agoktas@harran.edu.tr

¹ Department of Chemistry, Faculty of Science and Arts, Harran University, Sanliurfa 63290, Turkey

² Department of Mathematics and Science Education, Faculty of Education, Harran University, Sanliurfa 63290, Turkey

³ Department of Physics, Faculty of Science and Arts, Harran University, Sanliurfa 63290, Turkey

room temperature ferromagnetism (RTF) can be observed by substituting different transition metals, TM (TM = Mn, Fe, Co, etc.) within wide band gap ZnO semiconductors [6–8]. The reduction of the band gap dependent on the substitution of group B elements such as Mn, Fe, and Co, was reported by researchers due to the prevented electron–hole pair recombination through the generation of new energy levels [9–11].

To understand the influence of the strain presented within the film samples on their performance in applications, an extensive investigation has been done [12–14]. Most of the studies are focused on the variation within the structural, optical, and magnetic properties of the strained films. Some of them have reported improved optical properties of the films due to the strain/stress inside of the films [15, 16]. The change in the optical and magnetic properties of the film samples is possibly related to the variation within the crystal structure (lattice spacing and crystal anisotropy) and the additional stresses at the interface between the film sample and the sample holder [17, 18]. For instance, due to the relaxation of the residual stress of the SiO₂ thin films fabricated on a Si wafer, the reduction of the refractive index was reported [19]. The optical band gap widening in the indium-doped ZnO thin films produced on the silicon sample holder was also reported [20].

Inherently, ZnO has an n-type conductivity owing to the defect of oxygen deficiencies and zinc interstitials. Recently, a great deal of researchers has studied ZnO due to the above-mentioned superior properties with adjustable structural, optical, electrical, and magnetic characterizations by different metal dopants. Commonly, most researchers have chosen the TM group elements such as (Mn, Co, and Fe) to tune the magnetic properties of the ZnO nanostructures. For example, Sindhu et al. [6] reported RTF in Mn substituted ZnO (ZMO) depending on the precursor's concentration. Hadimani et al. [21] found an RTF within sol-gel spin-coated Zn_{1-x}Fe_xO (ZFO) thin films. RTF was observed in Co-doped ZnO (ZCO) nanoparticles synthesized by the solvothermal method [11]. To observe the RTF in TM substituted or doped ZnO thin films, the selection of the fabrication method as well as the film preparation conditions like molar concentration of precursor chemicals, annealing temperature/environments, and vacuum conditions are very crucial.

To synthesize the TM substitution or doping in ZnO thin films, various physical and chemical techniques such as thermal evaporation, magnetron sputtering, sol-gel spin coating method, chemical bath deposition (CBD), molecular beam epitaxy (MBE), spray pyrolysis, pulsed laser deposition (PLD) and successive ionic layer adsorption and reaction (SILAR) are needed. Among all, the wet chemical deposition (sol-gel) and the physical deposition (magnetron sputtering) techniques have some superior advantages. The first one is a relatively simple chemical solution-based technique,

requiring non-vacuum and low-cost equipment, including better stoichiometry control and relatively high homogeneity [22, 23]. On the other hand, the second one is a physical film growth technique, which can supply the high crystalline quality of thin films with high purity, uniform film thickness, required stoichiometry, and less roughness. Moreover, it provides the advantages of a high film-deposition rate, better reproducibility, and uniform separation within doped crystal lattice systems [24].

In the present study, Co, Mn, and Fe have been especially selected since some physical parameters (ionic radius, electronegativity, conductivity, etc.) are nearly like Zn and they can improve the structural, optical, and ferromagnetic properties of the ZnO host lattice positively [25, 26]. Therefore, to compare the effect of the strain and surface roughness including the film preparation methods on the structural, optical, and magnetic properties of the ZMO, ZCO, and ZFO, the samples were produced by chemical and physical techniques. To our best knowledge, there is a limited study comparing TM:ZnO thin films by different film growth techniques and the effect of the strain and surface roughness on certain physical characteristics of the TM-doped ZnO thin films. Therefore, it is worth comparing the structural, optical, and magnetic properties of the TM-doped ZnO thin films not only upon on the film preparation techniques but also on the strain and surface roughness of the films.

2 Experimental Methodology

2.1 Magnetron Sputter Deposited of TM: ZnO Thin Films

The nanostructured TM:ZnO (TM = Fe, Co, and Mn) thin films at certain doping levels (0–10 at%) were grown onto the soda lime glass (SLG) substrates by a magnetron-sputtering method and using ZnO (99.99%) metal target with some pieces of Mn₃O₄ (99.99%), α -Fe₂O₃ (99.99%) and Co₃O₄ (99.99%) sticking on the surface of the target. The doping concentration of the TM elements in the films was regulated by changing the number of pieces. Prior to the film growth, the vacuum chamber was shifted down to 5×10^{-3} Pa and fixed at 1 Pa during the film growth. To move out any surface contamination, the target was pre-sputtered for 10 min while the blind was inserted in place to avert the substrate from being deposited during the pre-sputtering. All the films ZFO, ZMO, and ZCO were produced on the SLG substrates at RT in the Ar environments for 30 min. During the pre-sputtering or sputtering process, the radio frequency energy of 200 W and argon of 5 sccm were used to fulfilling the film growth. Additionally, the produced films were annealed at 550 °C in an air atmosphere for 1 h.

2.2 Sol-Gel Growth of the TM-Doped ZnO Thin Films

To prepare the solution of TM-doped ZnO thin films, high purity $\text{Zn}(\text{NO}_3)_2 \cdot 6\text{H}_2\text{O}$, $\text{Co}(\text{NO}_3)_2 \cdot 6\text{H}_2\text{O}$, $\text{Fe}(\text{NO}_3)_3 \cdot 9\text{H}_2\text{O}$, and $\text{Mn}(\text{NO}_3)_2 \cdot 4\text{H}_2\text{O}$ precursor chemicals, were used as zinc (Zn), cobalt (Co), iron (Fe) and manganese (Mn) sources. 2-Methoxyethanol and ethanolamine were used as a solvent and a stabilizer, respectively. To regulate the molar doping ratio (0, 1, 2, 3, 5, and 10 at%) of the Mn, Fe, and Co the stoichiometric amount of each nitrate salt was dissolved in the 2-methoxyethanol by magnetic stirrer for 1 h at RT until to get a desired clear solution. The proper amount of ethanolamine was added to the mixtures to regulate the pH of the solutions (pH varied between 6.8 and 7.5). The total resultant mixture solutions were stirred at RT for 2 h to get homogeneous and transparent sols. After that, the final solutions were thoroughly stirred and aged overnight.

Before the dip coating process, the glass sample holders were cleaned with alcohol in ultrasonic baths. The cleaned sample holders were deposited via the dip coater system using the aged solutions. The deposited sample holders were preheated at 400 °C for 15 min and moved within the vertical oven under an air atmosphere with a constant withdrawal speed of 200 mm/s. To get the desired film thickness, the preheating and deposition processes were iterated 10 times. After that, the final preheated films were annealed at 550 °C for 1 h in an air environment.

2.3 Film Characterizations

A Rigaku Ultima III ($\text{CuK}\alpha$, 30 kV, 40 mA, 1.54 Å) x-ray diffraction (XRD) was performed to investigate the crystalline nature and crystal phase of the ZMO, ZFO, and ZCO nanocrystalline thin films. A field emission scanning electron microscopy (FESEM) (JEOL JSM-6700F) with an operating voltage of 30 keV and Hitachi5 model atomic force microscope were used to determine surface morphology/roughness, film thickness, particle size/shape, and the dispensation of particles on the film surfaces of the fabricated films. To detect the existence of the content atoms and their valence states, the x-ray photoelectron spectroscopy (XPS, PHI-5000 Versa probe, equipped with an Al $\text{K}\alpha$ x-ray radiation with the 1486.6 eV) was utilized.

The optical measurements of transmittance were done on a UV-Vis spectroscopy (Perkin Elmer spectrometer) for the wavelength range of 300–900 nm. To explore the magnetic characterization of the films, a vibrating sample magnetometer (VSM, Cryogenic Limited PPMS) was used in the temperature range of 5–300 K.

3 Results and Discussions

3.1 Surface and Stoichiometric Analysis

3.1.1 FESEM/AFM

The surface topography of the fabricated ZnO, Mn: ZnO, Co: ZnO, and Fe: ZnO films are presented in Fig. 1a–h for mean B group elements loading levels of 0 and 10 at%. As seen from Fig. 1a–h, all the film surfaces have dense, uniform, and homogeneous nanostructures (smooth surface) with polycrystalline nature and granular morphology, which have different grain shapes, exhibiting well crystalline quality films in all FESEM images. The different grain shapes are probably due to the use of different dopants and film growth techniques/conditions. Comparatively, the physically derived films are denser than those of the chemically derived films. However, they have relatively smaller grain sizes than the physically derived films. For both film growth techniques, the average grain size of the thin films is initially increased for the low doping ratio of (2 and 3 at%) TM and then decreased for the doping ratio of 5% TM. Among all the film samples, the 2% Fe-doped ZnO thin film has the highest grain size as seen in Fig. 1b and f. The cross-section images of the thin film samples have a 3 at% TM doping ratio, indicating that the film thicknesses vary approximately in the range of 400–410 nm. (In the film thickness' cross-section images (see Fig. 1), the Pa1 and Pa2 designs show the distance between the two points of film layers vertically, namely represents film thickness and the angle of film thickness, respectively).

The EDX spectrums of the chemically and physically fabricated films are presented in Fig. 2a and b, respectively, which demonstrate the presence of the different atoms in the produced film samples viz. Zn (appear around 1 keV, 8.6 keV, and 9.6 keV), Mn (appear around 0.4 keV, 5.8 keV, and 6.3 keV), Fe (appear around 0.7 keV, 6.4 keV, and 7.1 keV), Co (appear around 0.8 keV, 6.8 keV, and 7.5 keV), O (appeared around 0.5 keV), and Si (appeared around 1.8 keV). The Si peak was observed within the composition of the entire film sample since they have grown on the Si sample holder. The typical detection limit within the EDX analysis is around 0.5 at%. Furthermore, the doping content of the elements used is almost close to that used in the starting solutions according to the EDX analysis. So, the elemental constitution of the film samples is not anticipated to meet the respective levels in the precursor solution bath. This is likely because of the nucleation operation related to the thin film growth and the typically limited detection of the EDX tools.

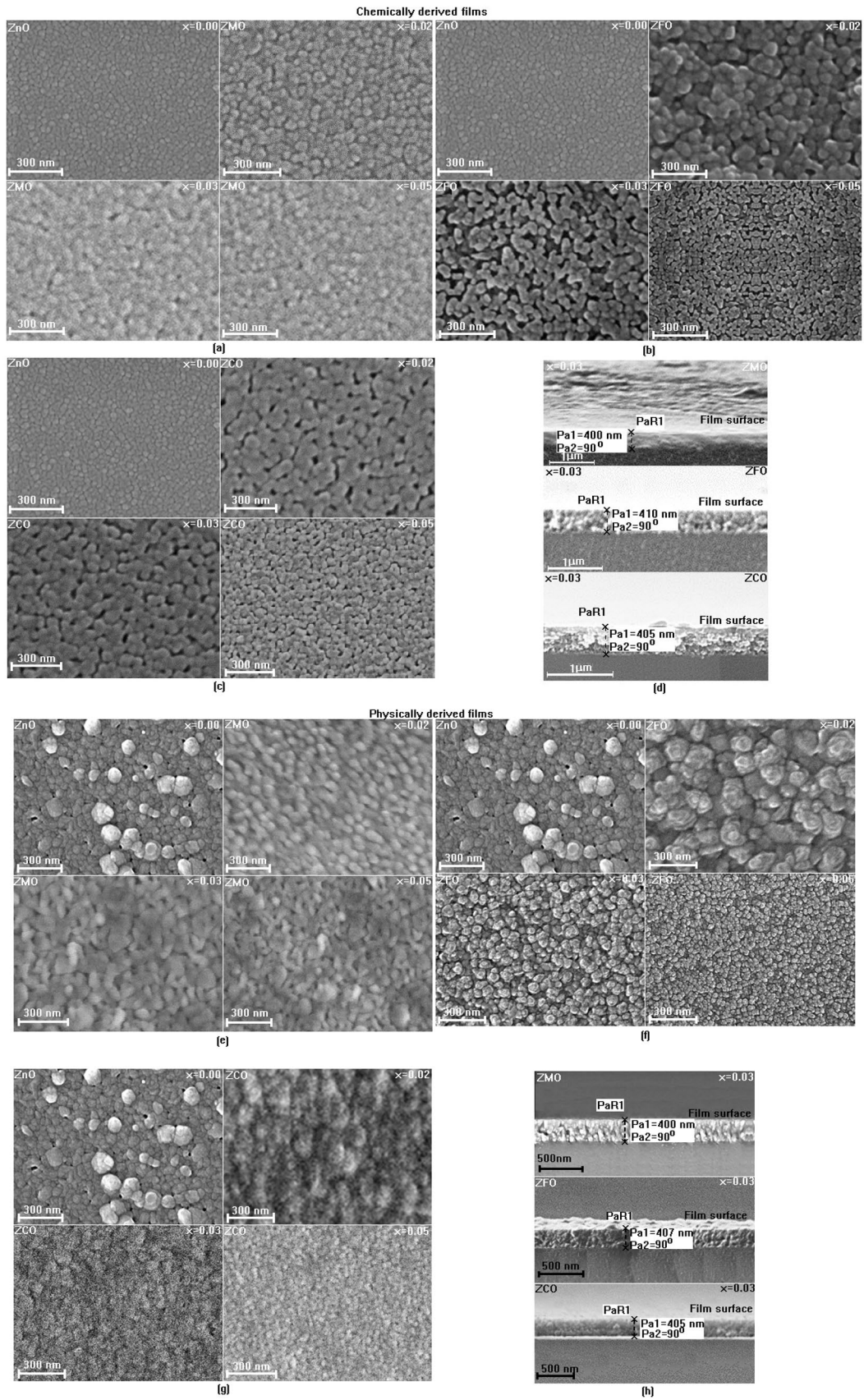


Fig. 1 FESEM images of chemically (a–d (average film thickness)) and physically (e–h (average film thickness)) derived and highly c-axis-oriented ZMO, ZCO, and ZFO films for the average doping levels of 0–5 at%

To get more information about the surface topography of the TM-doped ZnO, 3D AFM images showing the surface roughness and particle distribution over the film surfaces were given in Fig. 3a–e. Akin to FESEM images, it can be seen from Fig. 3a, b that the surface images of the film samples are inclusive of the randomly distributed nano-sized grains with different shapes, and they consist of uniform and dense surface particles without voids or porosity. The average surface roughness (R_a) of films was estimated at approximately 8.8–3.2 nm and 5.6–2.1 nm for the chemically and physically derived ZnO:TM films, respectively. It is observed that the R_a of the chemically derived ZnO:TM films is higher than those of the physically derived ZnO:TM films. Moreover, it is observed that the R_a has decreased with increasing TM-doping levels from 0 to 5%.

3.2 XPS Investigations

To get information about the binding energy and valance state of the alloying elements within the deposited, the XPS analysis is shown in Fig. 4 for the ZnO film samples containing 5 at% TM (TM = Mn, Co, and Fe) doping ratio. The inspection scan demonstrates that O, Fe, Co, Mn, and Zn are the main constituents within the films. Figure 5a showed that the binding energies were found around 1021.5 and 1044.5 (eV) energies corresponded to the Zn 2p_{3/2} and 2p_{1/2} summits. This outcome suggests that zinc has a valance state of 2+ since the bond energy position of the Zn 2p state is near the usual rate of zinc oxide [6]. In addition, the binding energy peaks shift within Zn 2p_{3/2} and 2p_{1/2} positions were observed on the way to higher eV (energy) worth by doping of Fe, Co, and Mn atoms in ZnO. This can be presumably ascribed to the partial substitution of Fe, Co, and Mn atoms within the ZnO lattice.

Bonding energies belonging to the Mn 2p_{3/2} and 2p_{1/2} tops were found around 641.6 and 653.4 eV as given in Fig. 5b. The noticed coincident power for the manganese loading endorses the existence of Mn, having valance state of 2+ within the zinc oxide [20]. Besides, the values of the binding energy of cobalt 2p_{3/2}, cobalt 2p_{1/2}, iron 2p_{3/2}, and iron 2p_{1/2} were found to be nearly 781 eV, 796 eV, 709.6 eV, and 722.4 eV, respectively (Fig. 5c, d). The obtained bonding energy values via XPS measurements propose a valance state of 2+ for the cobalt and iron. The noticed results are in good agreement with the literature [6, 21]. The enhanced peak strengths for the manganese, cobalt, and iron atoms are

possibly related to the corresponding doping ratios within the ZnO host.

3.3 Structure Properties

The corresponding x-ray diffraction patterns for the undoped zinc oxide and Zn_{1-x}TM_xO (TM = Mn, Co, and Fe) thin films grown on SLG sample holder at 300 K are given in Fig. 6a–c, with various Mn, Co, and Fe atoms doping ratios. Both the un-doped ZnO and Zn_{1-x}TM_xO samples show hexagonal wurtzite crystal structure (JCPDS card no. 01-071-5959) with strongly preferred orientation throughout the c-axis (002) and polycrystalline in nature. Similar crystal properties were also reported for the physically grown Zn_{1-x}Co_xO polycrystalline thin films [6]. No impurity phases related to Mn, Co, and Fe elements or compounds are observed at different average doping levels (0–10 at%) within the XRD detection limits, exhibiting that Mn²⁺, Co²⁺, and Fe²⁺ could substitute for Zn²⁺ or incorporate into interstitial sites in the ZnO lattice.

According to the XRD measurements (Fig. 6a–f), the disparity for the (002) height strength varies alike Co, Fe, and Mn loadings, reflecting it firstly enhances via loading contents up to the optimal level; after that, it reduces dramatically through the enhancement in loading content compared with the ZnO, except for the derived ZFO and ZMO thin films. Scherrer's formula was used to calculate the crystallite sizes (D_{hkl}) of un-doped and TM-doped ZnO thin films. The crystallite size of the samples differs from one another depending on the dopant atoms. In comparison to the undoped zinc oxide thin film, the peak intensities of the (002) miller plane corresponded for ZMO, ZFO, and ZCO film samples have relatively depressive merits as seen in Table 1. In the case of Co, Fe, and Mn loadings, the peak intensities of (002) miller plane of the film samples reduce proportionally as TM loading ratio excluding for 3% and 5% B group metal doping level within the iron-doped zinc oxide films. The noticed decline in TM:ZnO films were also described for Zn_{1-x}Mn_xO [2], Zn_{1-x}Co_xO [6], and Zn_{1-x}Fe_xO [20] thin film samples. The variant in the orientation degree of the c-axis and D_{002} is chiefly caused by used film production techniques and preconditions [6, 22].

As can be seen in Table 1, the lattice constant (c) of the ZMO and ZFO films enhances as B group metal loading levels, which is due to the doping of Mn²⁺ or Fe²⁺ for Zn²⁺ locations within the zinc oxide as the ionic radii of Mn²⁺ (0.80 Å) or Fe²⁺ (0.74 Å) is comparatively higher than that of Zn²⁺ (0.72 Å). These outcomes were previously published in refs. [2, 21, 26]. Besides, the cobalt-doped zinc-oxide thin films have not shown a distinguished variance c likely because of the little distinction between the anion radii of Zn²⁺ (0.60 Å) and Co²⁺ (0.58 Å) in a tetrahedral ordering.

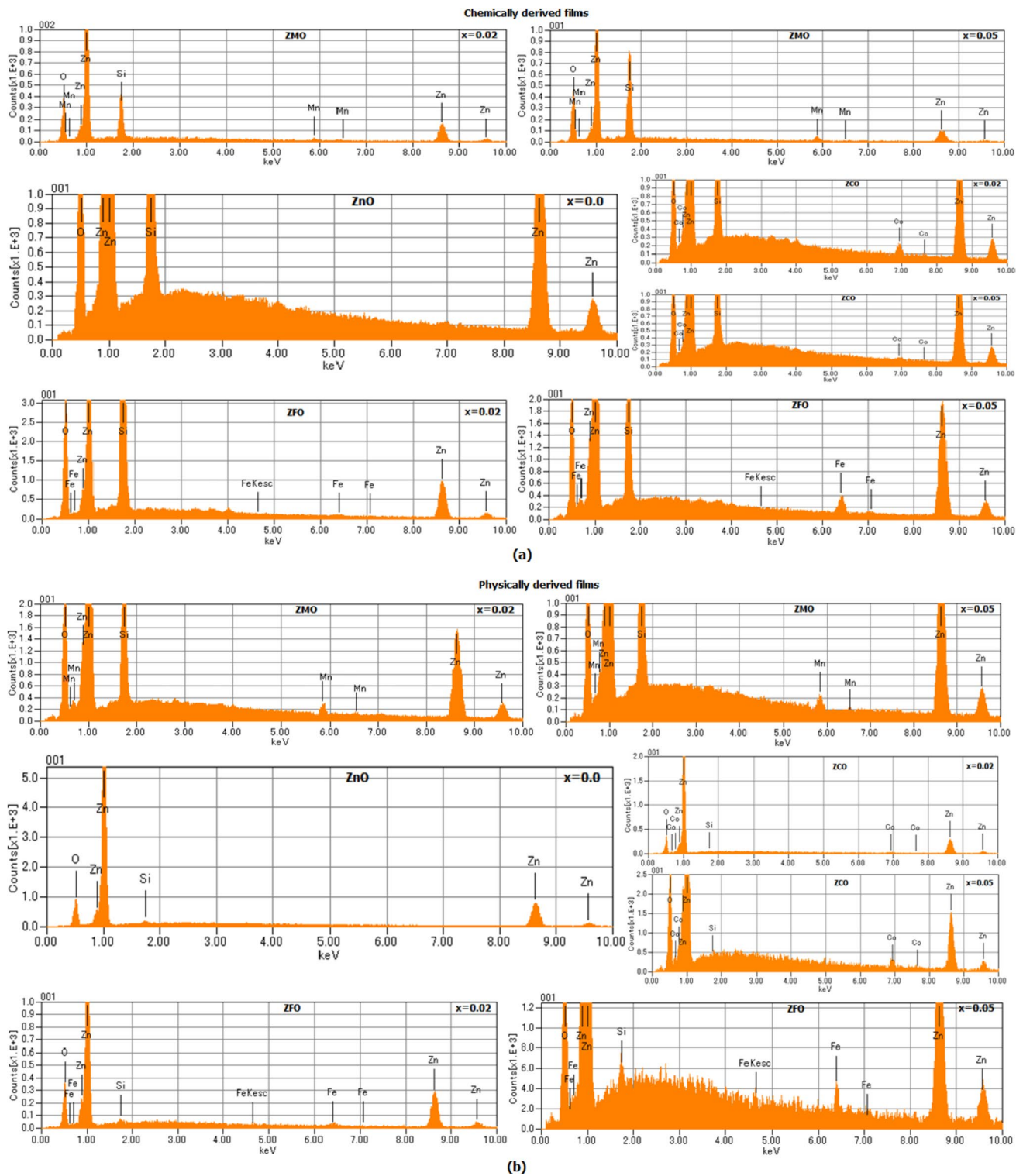
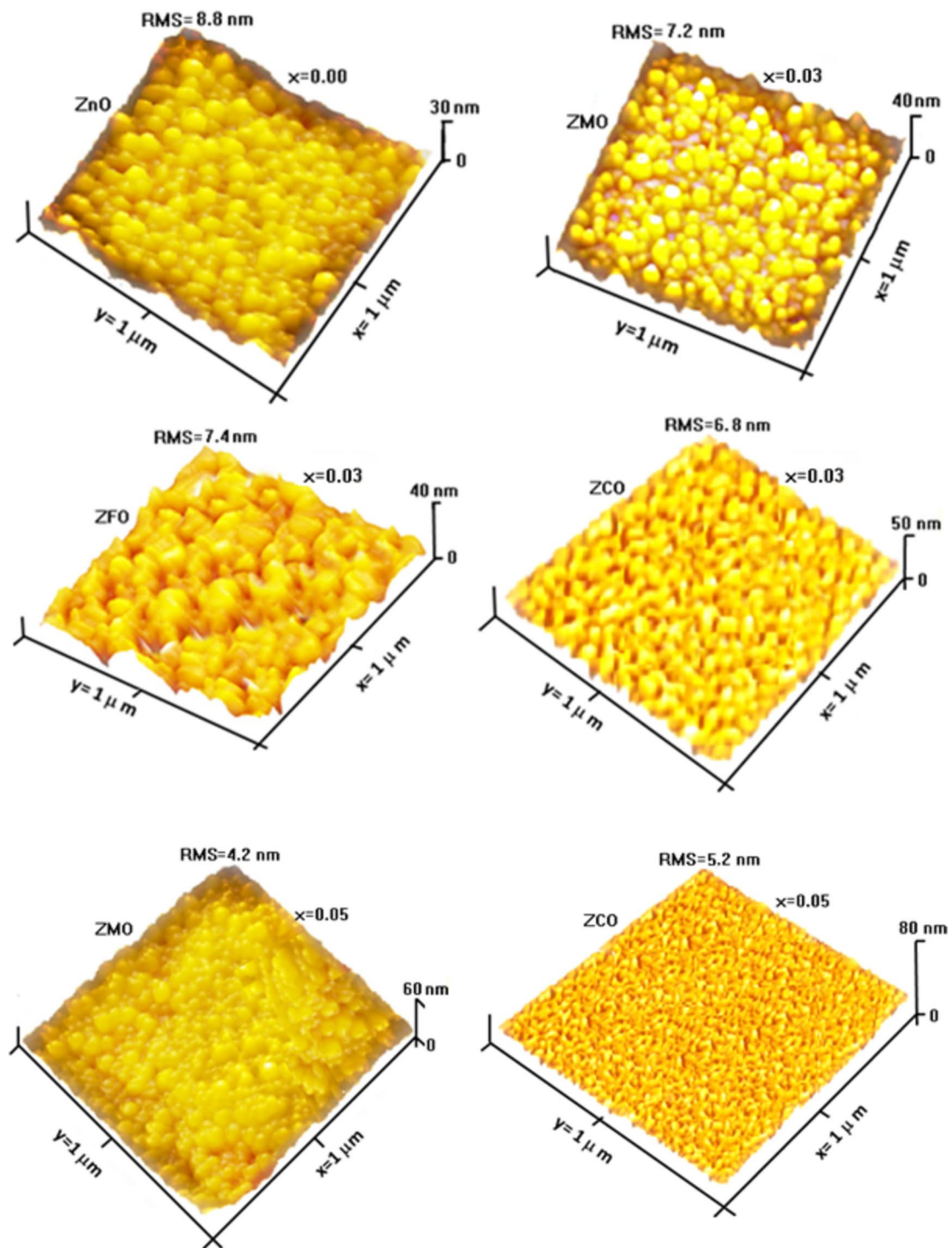


Fig. 2 The EDX 3D images of the chemically (a) and physically (b) derived and highly c-axis-oriented ZMO, ZCO, and ZFO films for the average doping levels of 0–5 at%

The noticed result is harmonious with the literature reported in refs. [6, 24, 25].

In the case of both film types, the influences of the strain and the deviation linear thermal expansion coefficient (α) of zinc

oxide-based thin films ($7 \times 10^{-6}/^{\circ}\text{C}$) and SLG ($9 \times 10^{-6}/^{\circ}\text{C}$), as well as fretwork flaws with various cation size because of the film growth conditions and the doping of B group elements into ZnO. These influences cannot be ignored [2, 4, 6].



a

Fig. 3 AFM 3D images of the chemically (a) and physically (b) derived and highly c-axis-oriented ZMO, ZCO, and ZFO films for the average doping levels of 0–5 at%

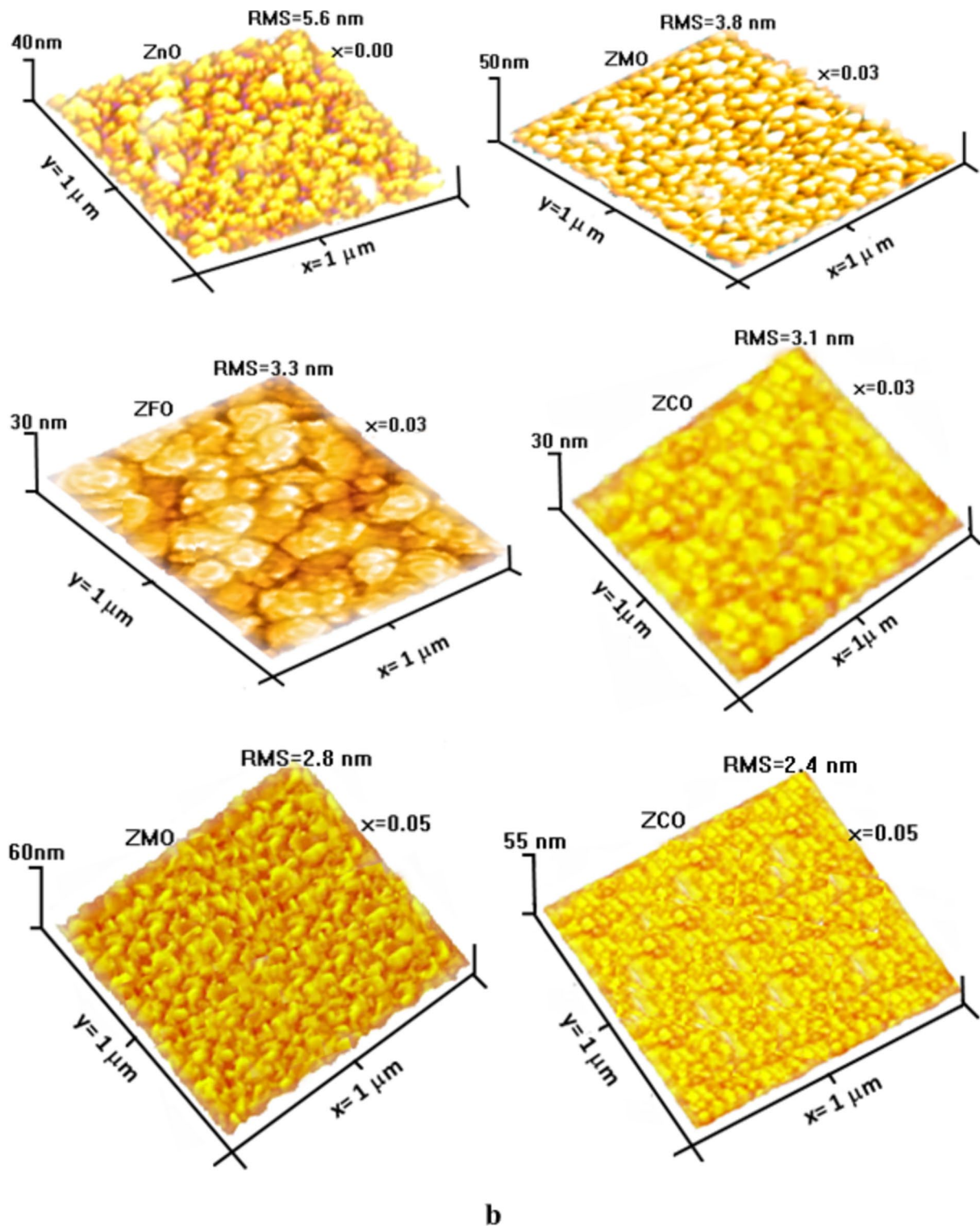


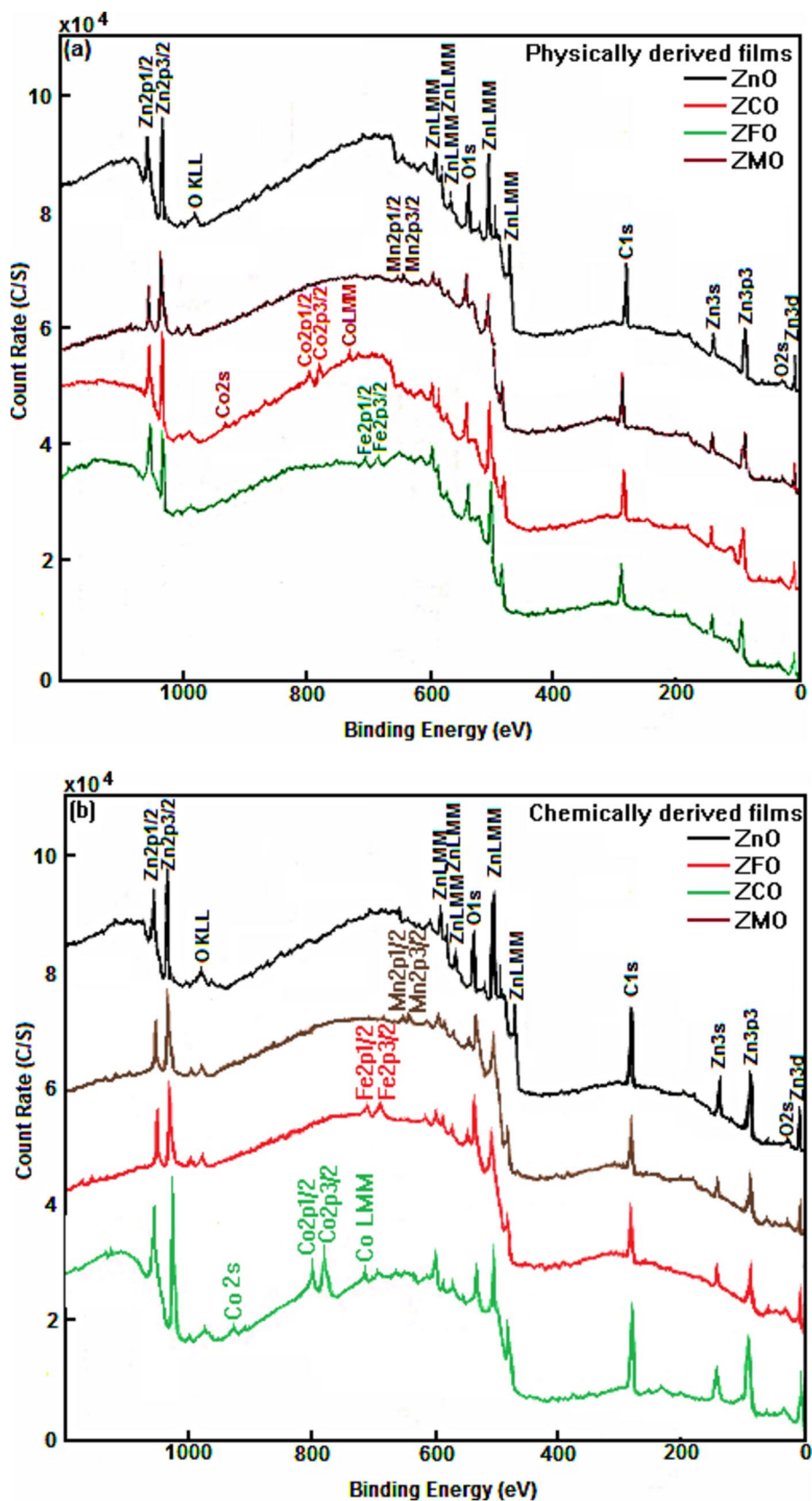
Fig. 3 (continued)

3.4 Optical Studies

The transmittance spectra of ZnO and TM:ZnO (TM = Mn, Co, and Fe) thin films in the range from 300 to 800 nm are

given in Fig. 7a–f. The observed intervention perimeter in spectrums exhibits well thin film grade in both film preparation methods. Compared to undoped ZnO, it is worth noting that at low metal doping concentrations (1–3 at% Mn,

Fig. 4 XPS spectrums of the chemically (a) and physically (b) derived and highly c-axis-oriented ZMO, ZCO, and ZFO films for the average doping levels of 0 and 5 at%



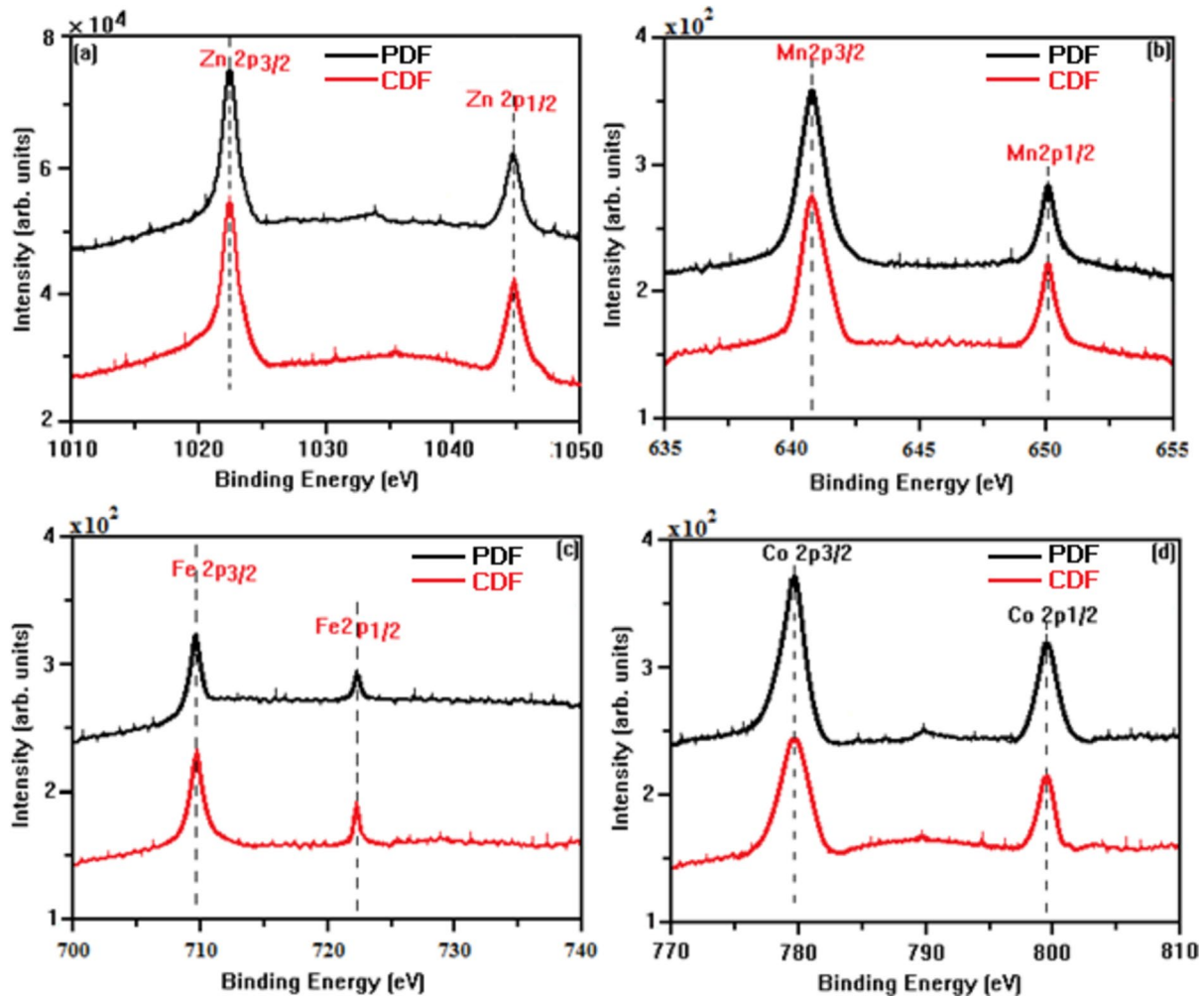


Fig. 5 Wide-scan XPS spectra of the chemically and physically derived and highly c-axis-oriented ZMO, ZCO and ZFO films for the core level of the Zn2p (a), Mn2p (b), Fe2p (c), and Co2p (d) and doping level 5 at%

Co, and Fe), ZnO thin films demonstrate peak transparency (above 80%) in the visible span for all film samples except for the physically derived ZCO thin films. In the company of all ZnO and B-group metal-doped zinc oxide films, the ZnO:Fe film has exhibited high transparency within the Vis (visible) scale, likely related to the high film quality as observed in XRD analysis rather than observed high RMS. Considering the extra TM-doped ZnO films, the transparency is reduced by the enhancement of the TM doping ratio. Among all, both physically and chemically fabricated ZCO films relatively demonstrate the lowest transparency approximately lower than 65% in the Uv span (see Fig. 7e and f), especially at high doping levels (> 3 at%). The observed findings are in good agreement with the previously reported investigations on similar film samples [24, 27, 28].

In general, it is observed that the chemically derived ZnO:TM films have a higher transmittance than those of physically derived ZnO:TM films. However, the RMS of the

physically derived ZnO:TM films is less than those of the chemically derived ZnO:TM films (Table 1). This situation can be explained by the top film status of the chemically derived TM:ZnO thin films. This observed high transparency and crystallinity as well as the relatively low RMS make these materials a good candidate for optoelectronic devices.

The forbidden band gap energy (E_g) of the thin films is approximately obtained by Tauc's equation [4]. With a forecast of the horizontal section of a curve of $(\alpha h\nu)^{1/2}$ on the y-bloc contrast $E_g (h\nu)$ on the x-bloc provides the utility of the E_g , whereas $(\alpha h\nu)^{1/2} = 0$. Considering this concept, the E_g of TM:ZnO films was assessed as presented in Fig. 8a–f. The optical E_g values of both film preparation techniques were changed according to the TM doping level and film preparation methods as seen in Figs. 8a–f. Pure ZnO has the E_g of values of about 3.23 and 3.3 eV for the chemical and physical film production techniques, respectively. The small difference of the 0.07 eV is likely due to the film

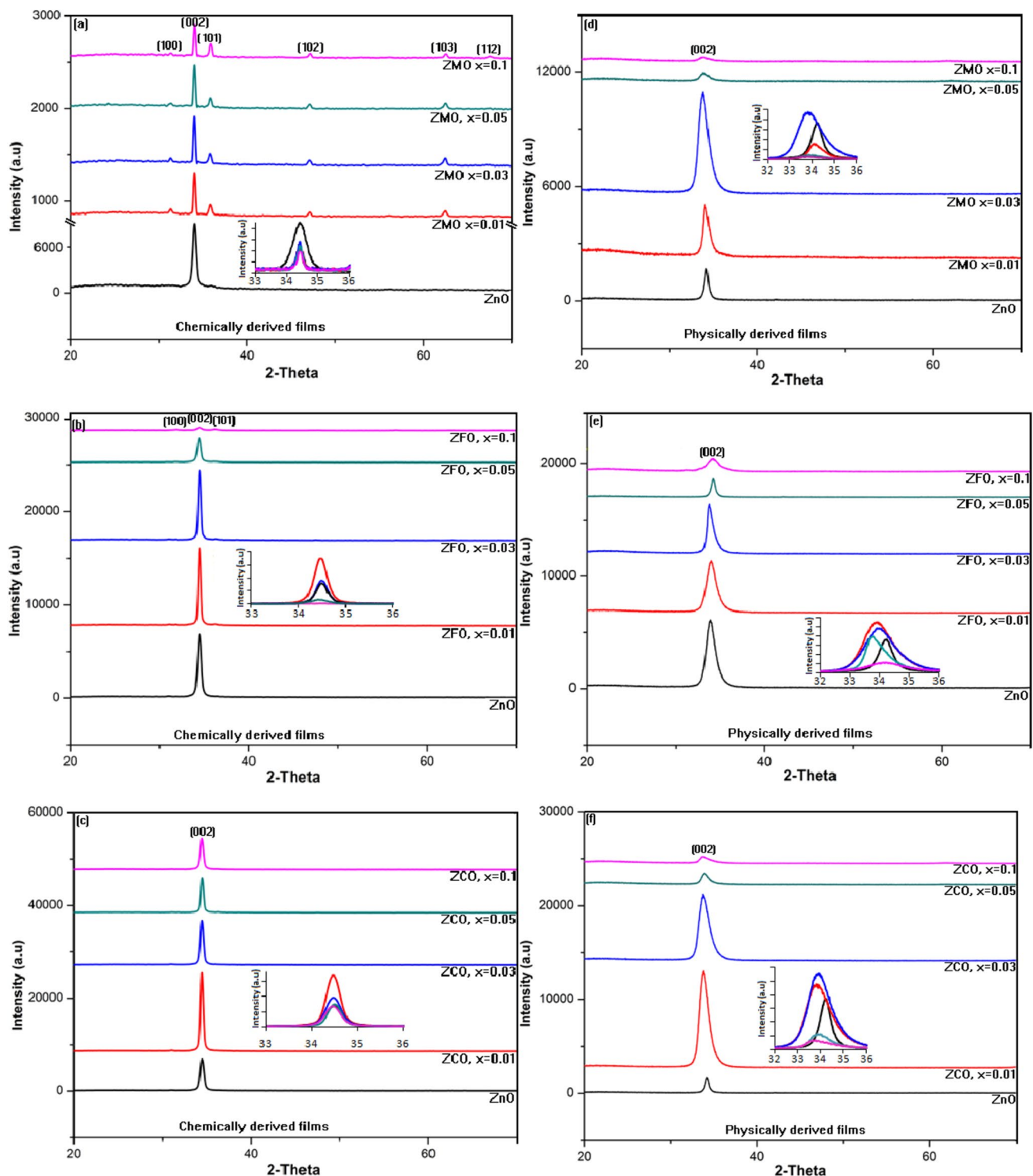


Fig. 6 XRD spectra of chemically (a–c) and physically (d–f) derived and highly c-axis-oriented ZMO, ZCO and ZFO films for the average doping levels of 0–5 at% (insets: wide-range XRD spectra of corresponding ZnO: TM films)

preparation conditions leading to different film crystallization degrees and the formation of the defects [29].

With the doping of the TM elements, the E_g of the film samples has shown the same shift (blue or red) trend

for the same ZnO:TM and film preparation technique. For instance, the E_g values of the physically and chemically produced ZFO/ZCO thin film samples were monotonically reduced (redshift) by the enhancement in Fe or

Table 1 Summary of structural and morphological characteristics in the chemically (a, b, and c) and physically (d, e, and f) derived and highly c-axis oriented ZMO, ZCO, and ZFO films for the average doping levels of 0–10 at %

Chemically derived thin films							
Film type	TM ratio (%)	FWHM (β°)	2θ (deg.)	D (nm) ₀₀₂	c (\AA)	Strain, $\epsilon \times 10^{-3}$	RMS (nm)
ZnO	0.0	0.70	34.46	12	5.207	2.95	8.8
ZMO	1.0	0.35	34.36	24	5.222	1.46	8.5
ZMO	3.0	0.30	34.38	28	5.219	1.25	7.2
ZMO	5.0	0.37	34.40	23	5.216	1.56	4.2
ZMO	10.0	0.45	34.42	16	5.213	1.90	3.8
ZFO	1.0	0.35	34.44	24	5.210	1.46	6.8
ZFO	3.0	0.27	34.42	31	5.213	1.12	7.4
ZFO	5.0	0.76	34.36	11	5.222	3.17	5.4
ZFO	10.0	1.65	34.32	5	5.223	6.87	9
ZCO	1.0	0.60	34.36	14	5.222	2.50	7.1
ZCO	3.0	0.65	34.34	13	5.225	2.70	6.8
ZCO	5.0	0.62	34.42	13.5	5.212	2.58	5.2
ZCO	10.00	0.74	34.30	11.3	5.231	3.08	4.6
Physically derived thin films							
Film type	TM ratio (%)	FWHM (β°)	2θ (deg.)	D (nm) ₀₀₂	c (\AA)	Strain, $\epsilon \times 10^{-3}$	RMS (nm)
ZnO	0.0	0.40	34.20	21	5.238	1.67	5.6
ZMO	1.0	0.65	34.04	13	5.263	2.71	3.1
ZMO	3.0	1.40	33.82	6	5.296	5.86	3.8
ZMO	5.0	1.80	33.80	5	5.300	7.53	2.6
ZMO	10.0	2.0	33.78	4	5.303	8.36	2.1
ZFO	1.0	1.10	33.82	7.6	5.296	4.60	3.0
ZFO	3.0	0.86	33.64	9.8	5.324	3.26	3.3
ZFO	5.0	0.68	33.88	12.4	5.287	2.84	2.8
ZFO	10.0	1.40	34.12	6	5.250	5.83	2.6
ZCO	1.0	0.94	33.92	8.9	5.281	3.92	3.7
ZCO	3.0	1.02	33.85	8.2	5.292	4.26	3.1
ZCO	5.0	0.86	33.74	9.8	5.309	3.59	4.2
ZCO	10.00	1.60	33.72	5.3	5.312	6.68	2.5

Co doping level. On the other hand, it has observed an enhancement of the E_g values (blue shift) of physically and chemically produced ZMO thin films. The observed redshift within the E_g values for the ZnO:TM film samples could be expressed via sp–d interchange interplay, exhibiting a powerful interconnection offer between the d shell electron of transition metals, and the s and p shell electrons of the host zinc oxide [2, 4, 24]. Moreover, the quantum confinement effect in nanosized structures, the impurity levels, and the structural parameters also corresponds to the band gap narrowing. Nonetheless, the widening of the E_g corresponding to the ZnO:Mn films is possibly related to the larger E_g (4.2 eV) energy of manganese oxide or Burstein Moss phenomena [29, 30]. The observed outcomes are in good accordance with published investigations about the ZnO:Mn [2, 28], ZnO: Fe [4, 26, 29], and ZnO:Co [24, 28, 29].

3.5 Magnetic Properties

Magnetic characterization of the fabricated ZnO and ZnO:TM thin films was explored at room temperature (300 K) and magnetic field (H) range of ± 10 kOe employing a SQUID magnetometer with H parallel to the film plane. The diamagnetic contribution of the glass substrate was accordingly removed from the background data as done in previous reports [24, 30]. Figure 9a–f demonstrates the magnetization (M) versus H (Oe) curves of the zinc oxide and TM:ZnO films at 300 K regarding the various loading ratio (0–5 at%). The M – H curves of pure ZnO have paramagnetic behavior and the other film samples have a ferromagnetic response as they represent the hysteresis loop for the chemically and physically derived ZnO:Mn and ZnO:Fe thin films except for the ZnO:Co thin films. The origin of the observed room temperature ferromagnetism (RTF) and

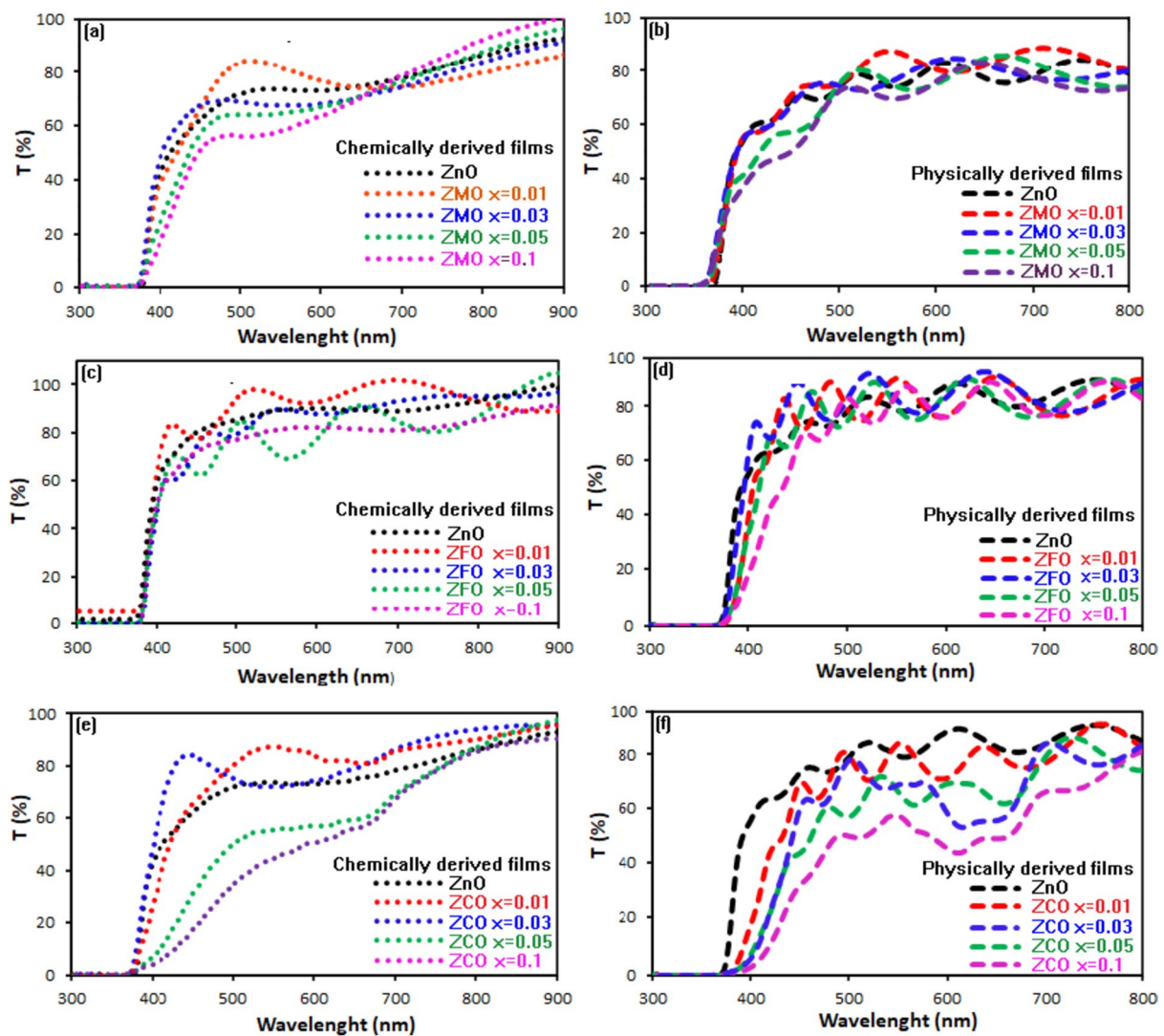


Fig. 7 Transmittance of spectra of chemically (a–c) and physically (d–f) derived and highly c-axis-oriented ZMO, ZCO, and ZFO films for the average doping levels of 0–10 at%

paramagnetism for the chemically and physically produced ZMO, ZFO, and ZCO thin films will be separately discussed and compared below, respectively.

As seen in Fig. 9a and d, among the ZnO:Fe thin films, the high ups the ferromagnetic response in the case of the loading ratio of 5 at% Mn, which is due to enhanced magnetic moment interaction via enhanced Mn clustering and doping level. Comparatively, the highest ferromagnetic response was observed for the physically derived ZMO films. This may be also related to the higher homogeneity of the physically derived films, leading to a more magnetic moment interaction compared to the chemically derived films. The observed RTF in ZnO:Mn (1–5 at% Mn) thin films was consistent with Mn-doped ZnO thin films derived via RF magnetron sputtering [31–33] and thermal evaporator [34] methods. However, it is reported in ref. [35] that

the highest ferromagnetic response for the Mn-doped ZnO film with 2.2 at% loading level and the observed ferromagnetic response decrease as the Mn doping ratio enhances. The observed contradiction with the present study could be expressed using film preparation technique and starting chemicals as well as preparation conditions, which resulted in different characterizations and results.

The origin of the observed RTF in ZMO cannot be attributed to the presence of the secondary phases (Mn, MnO, MnO₂, Mn₃O₄, and ZnMn₂O₄) since none of them has not been observed in the XRD, EDX, and XPS analysis. In addition, many of them have an antiferromagnetic nature except for Mn₃O₄, which has a Curie temperature (T_C) of 50 K [36–38]. Furthermore, the standard superchange or double-exchange (DE) interaction as well as the Ruderman–Kittel–Kasuya–Yosida (RKKY) mechanism

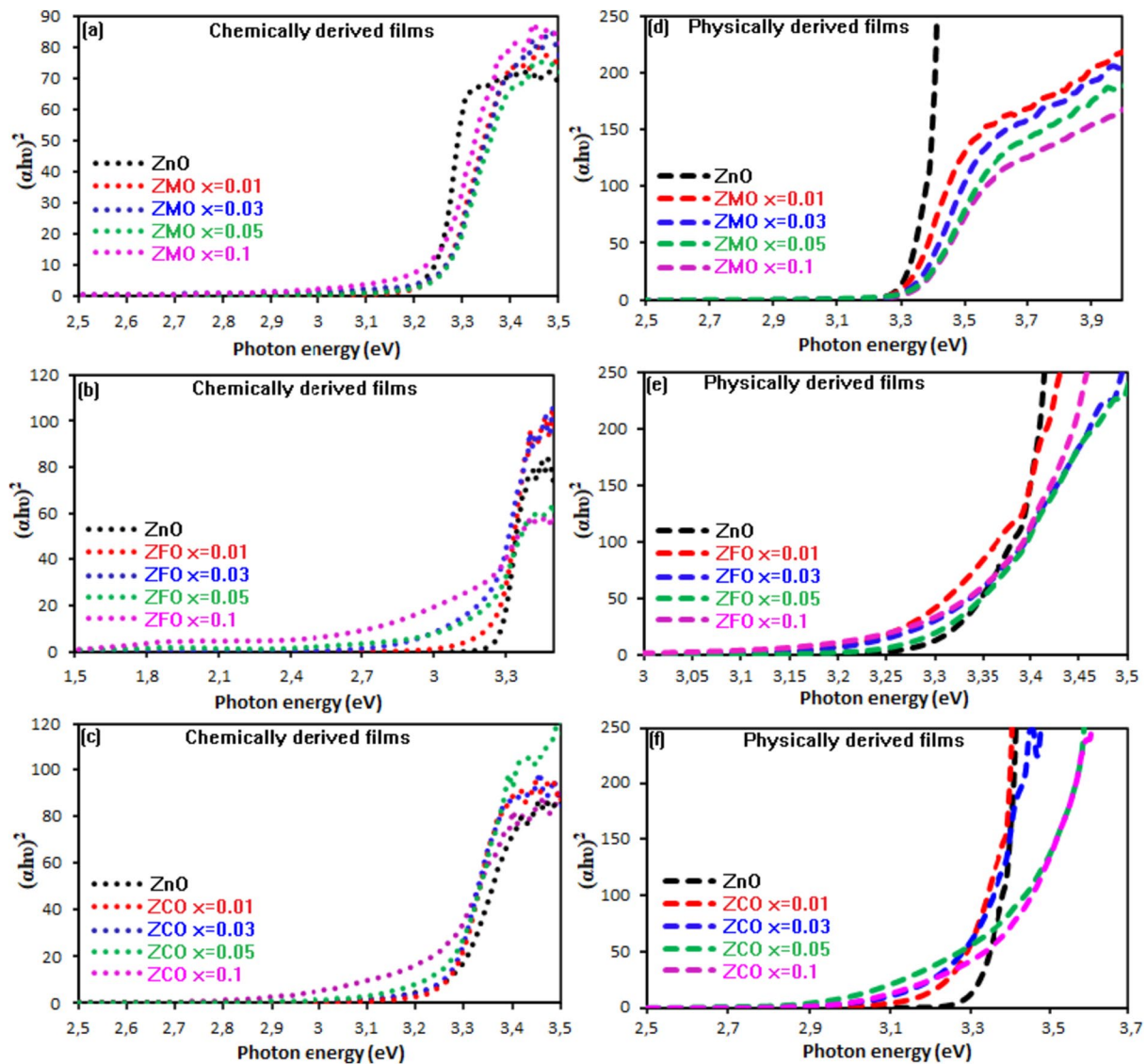


Fig. 8 Plot of $(\alpha h\nu)^2$ vs. $h\nu$ for the chemically (a–c) and physically (d–f) derived and highly c-axis-oriented ZMO, ZCO, and ZFO films for the average doping levels of 0–10 %

cannot result in long-range magnetic order at low concentrations of magnetic ions. Moreover, as discussed in many recent studies, the origin of the RTF in ZMO may be related to the defects-induced RTF and oxygen vacancies, etc. [38–40]. However, in presenting ZMO thin films, it is not possible that the resistivity of the samples is high ($> 105 \Omega \cdot \text{cm}$ at room temperature) and the oxygen vacancies have not been observed in XPS. Therefore, the only fact is that the origin of the RTF is possibly due to the intrinsic behavior of the ZMO.

Compared to the physically derived ZFO thin films, a clear and exact hysteresis, as well as a higher ferromagnetic response, was observed for the chemically derived films at room temperature (Fig. 9b and e). This may be related to the relatively higher crystallization of the chemically derived ZFO thin films. The observed reduction in ferromagnetic

response by the enhanced Fe doping level could be attributed to the addition of more Fe atoms leading to more strain and low crystallization, blocking Fe–Fe magnetic moments interaction (see Table 1). The observed root of the RTF in ZFO thin films can be explained based on the intrinsic ferromagnetism, parasitic phases viz. FeO, $g\text{-Fe}_2\text{O}_3$, Fe_3O_4 , $\text{Fe}_{3-x}\text{Zn}_x\text{O}_4$ and ZnFe_2O_4 , Fe clusters, and (iv) defects in the ZFO system [40]. The ferromagnetism convinced via electrons or holes (RKKY or DE interaction) for the films having a high doping ratio of TM as Fe (> 10 at%) cannot be connected to the observed RTF in ZFO because of the low doping level of the Fe. Impurity phases like FeO and ZnFe_2O_4 have an antiferromagnetic nature having a Neel temperature (T_N) of 291 and 10 (+1 or –1) K, respectively [2, 41], whereas $g\text{-Fe}_2\text{O}_3$ and Fe_3O_4 have a ferromagnetic

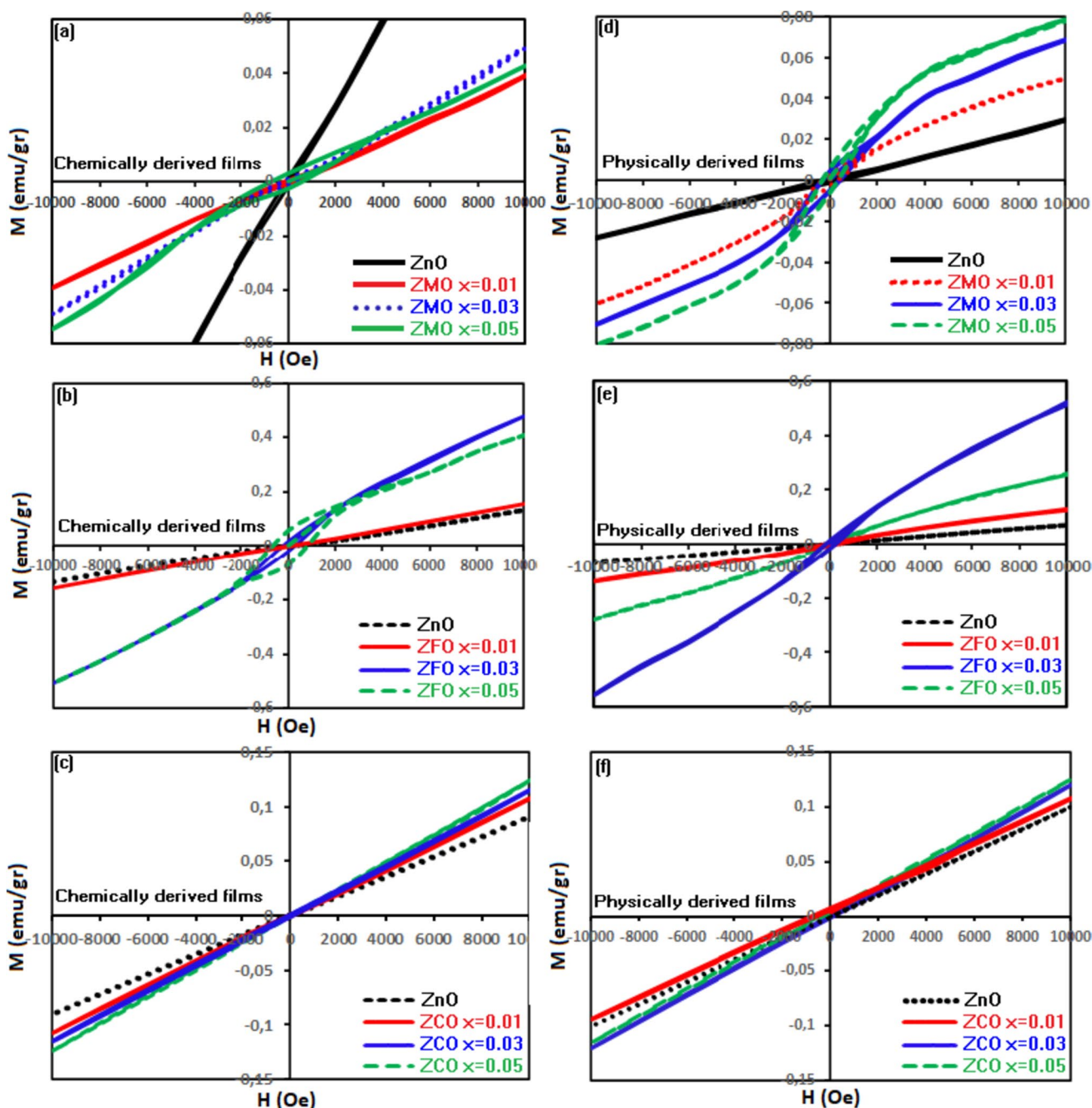


Fig. 9 Magnetic field dependent M-H hysteresis curve of the chemically (a–c) and physically (d–f) derived and highly c-axis-oriented ZMO, ZFO, and ZCO films for the average doping levels of 0–5 at%

response with high T_C of 873 and 858 K, respectively [2, 21]. None of them can be the reason for RTF in ZFO thin films, since they have not been found in the XRD, SEM, and XPS analysis. So, it is concluded that the origin of the observed RTF in ZFO thin films is likely due to the intrinsic nature of the high-quality chemically and physically fabricated thin films.

It is interesting that both chemically and physically derived ZCO thin films have paramagnetic responses at 300 K. This

could be expressed via the isolated Co-free spins. Similar findings were also reported for the $Zn_{1-x}Co_xO$ nanopowder synthesized by the rheological phase reaction-precursor technique [42] and for the Co-doped ZnO thin films prepared by the PLD technique [43]. They expressed this fact as the result of the non-coupled interaction between Co^{2+} ions due to the absence of segregated magnetic Co^{2+} ions. Moreno et al. [44] also reported that there was no ferromagnetic nature with a smaller paramagnetic contribution than that of diamagnetic

signals for the Co-doped ZnO thin films. The main cause of this behavior was commended and assigned for the evaluation of non-magnetic Co-Zn-O compounds as imperfections. Moreover, Cong et al. [42] and Belgazi et al. [45] observed the paramagnetic nature of the Co-doped ZnO thin films derived from in-spray pyrolysis (SP) technique. However, the recent available scientific information about the Co-doped ZnO thin films was opposed. For instance, Polat et al. [46] observed RTF in ZnO:Co thin films derived by the PLD method and annealed in an oxygen-deficient environment. In addition, the $Zn_{1-x}Co_xO$ thin films are synthesized via the SP method in air ambiance [47]. The result of this study showed that the film samples had a ferromagnetic nature at 300 K. Therefore, these conflicts reflect the employed film preparation methods and synthesis orders are the main factors that impact the magnetic behavior of the ZnO:Co thin films.

To discuss the origin of the observed paramagnetic nature, the following are commended: (i) For the presented films, the impurities cannot be the reason for the observed RTF paramagnetism since they have not been found within the XRD, SEM, or XPS measurements and also they have ferromagnetic (Co, $T_C = 1373$ K), antiferromagnetic (CoO, Neel temperature (T_N) = 291 K), non-magnetic (Co_2O_3), antiferromagnetic (Co_3O_4 , $T_N = 40$ –50 K) and spinel ferromagnetic ($ZnCo_2O_3$, $T_C = 2/3$ K) nature generally; (ii) The main theoretical interactions (RKKY or DE) in DMS governing the RTF can be easily eliminated due to the used relatively low TM doping levels ($0 \leq x \leq 5$ at%); and (iii) the magnetic bond polarons due to the interaction between the oxygen vacancies acting as shallow donors and Co^{+2} ions cannot be addressed as the observed paramagnetic nature of the ZCO at room temperature. Therefore, due to the abovementioned reasons and facts, the paramagnetic nature of physically and chemically derived ZCO films is possibly attributed to the non-magnetic nature of CoO or the imperfection in the form of the Zn-Co-O, which cannot be detected by XRD, SEM, or XPS analysis likely because of its very small nano-sized forms.

4 Conclusions

ZnO and transition metal (TM = Mn, Co, and Fe)-doped ZnO nanostructured thin films, which are highly transparent, well crystallized, and have ferromagnetic properties at room temperature, were successfully produced by chemical and physical methods at various TM doping concentrations of 0–10 at%, and an average film thickness of 400 nm. Comparatively, higher crystallization and orientation were observed in chemically derived ZnO:TM thin films, which had hexagonal

wurtzite phases along the (002) Miller plane, than those of physically derived films. FESEM and AFM surface analysis exhibited that the homogeneous and dense surface morphology with the randomly scattered grains and their size and shape varied with respect to the synthesizing way and TM doping ratio. EDX and XPS analysis confirmed the presence of the Mn^{2+} , Fe^{2+} , and Co^{2+} within the host ZnO lattice. It was generally observed that the optical transmission of the chemically derived ZnO:TM thin films was higher than those of the physically produced films and the highest values of transmittance were observed at low TM doping rates. The variation of the optical band gap of films derived by both techniques was in good harmony with each other except for the ZMO films.

Magnetic measurements showed that the chemically and physically derived ZMO or ZFO films had room temperature ferromagnetism, addressed as intrinsic behavior of the films, while ZCO films were shown room temperature paramagnetism. The observed ferromagnetic and paramagnetic strengths were monotonically varied according to the preparation route and the TM doping level. Amongst all, the highest ferromagnetic response was found for the chemically and physically ZFO thin films. This nature can be attributed to the high crystalline quality and excellent interaction of Fe^{2+} – Fe^{2+} magnetic moments of the ZFO.

XPS analysis technique outcomes have clearly proved that the doping of Mn^{2+} , Fe^{2+} , and Co^{2+} have successfully unified within the ZnO wurtzite lattice at the Zn^{2+} sites for all the fabricated films. The observed results are in good agreement with the reported structural, optical, and magnetic characterizations of the various ZnO:TM thin films synthesized via different techniques. Nonetheless, the presented investigation demonstrates the first detailed description comparative study about chemically and physically fabricated TM:ZnO by utilizing sol-gel dip coating and magnetron-sputtering routes and scrutinizing the influence of the various TM elements on the structural, optical, and magnetic characterization of the ZnO nanostructured thin films. Furthermore, the fabricated films by both techniques are relatively homogeneous and have high quality in terms of optical and crystallization degree. Moreover, the produced films have huge potential for optoelectronic, spintronic, and photocatalytic applications running at room temperature.

Funding This study was performed in Harran University and supported by the Scientific and Technological Research Council of Harran University (HUBAK) with project number 21087.

Declarations

Conflict of Interest The authors declare no competing interests.

References

- Ilyas, U., Rawat, R.S., Roshan, G., Tan, T.L., Lee, P., Springham, S.V., Zhang, S., Li Fengji, R., Chen, H.D.: Sun Quenching of surface traps in Mn doped ZnO thin films for enhanced optical Transparency. *Appl. Surf. Sci.* **258**, 890 (2010)
- Goktas, A., Aslan, F., Yeşilata, B., Boz, İ.: Physical properties of solution processable n-type Fe and Al co-doped ZnO nanostructured thin films: role of Al doping levels and annealing Mater. Sci. Semi. Proces. **75**, 221 (2013)
- Merdes, S., Ziem, F., Lavrenko, T., Walter, T., Lauer mann, I., Klingsporn, M., Schmidt, S., Hergert, F., Schlatmann R.: Above 16% efficient sequentially grown Cu(In,Ga)(Se,S)2-based solar cells with atomic layer deposited Zn(O,S) buffers. *Prog. Photovolt: Res. Appl.* **23**, 1493 (2015)
- Goktas, A., Tumbul, A., Aba, Z., Durgun, M.: Durgun Mg doping levels and annealing temperature induced structural, optical and electrical properties of highly c-axis oriented ZnO:Mg thin films and Al/ZnO:Mg/pSi/Al heterojunction diode. *Thin Solid Films* **680**, 20 (2019)
- Anandan, S., Miyachi, M.: Ce-doped ZnO (CexZn1-xO) becomes an efficient visible-light sensitive photocatalyst by co-catalyst (Cu2+) grafting. *Phys. Chem. Chem. Phys.* **13**, 14937 (2011)
- Sindhu, H.S., Rajendra, B.V., Kulkarni, S.D., Babu, P.D.: Optical, electrical and magnetic properties of fiber structure Zn0.99Mn0.01O films prepared by spray pyrolysis. *Thin Solid Films* **655**, 83 (2018)
- Avrutin, V., Izyumskaya, N., Ozgur, Ü., Silversmith, D.J., Morkoc, H.: Ferromagnetism in ZnO-and GaN-based diluted magnetic semiconductors: achievements and challenges. *Proc. IEEE* **98**, 1288–1301 (2010)
- Hadimani, P.L., Ghosh, S.S., Sil, A.: Preparation of Fe doped ZnO thin films and their structural, magnetic, electrical characterization. *Superlatt. Microstruc.* **120**, 199 (2018)
- Achouri, F., Corbel, S., Balan, L., Mozet, K., Girot, E., Medjahdi, G., Ben, M., Ghrabi, A., Schneider, R.: Porous Mn-doped ZnO nanoparticles for enhanced solar and visible light photocatalysis. *JMADE* **101**, 309 (2016)
- Goktas, A., Mutlu, İ.H.: Structural, optical, and magnetic properties of solution-processed co-doped ZnS thin films. *J. Elect. Mater.* **45**, 5709 (2016)
- Aghagoli, Z., Ardyanian, M.: Synthesis and study of the structure, magnetic, optical and methane gas sensing properties of cobalt doped zinc oxide microstructures. *J. Mater. Sci. Mater. Electron.* **29**, 7130 (2018)
- Zarbalı, M., Gökteş, A., Mutlu, İ.H., Kazan, S., Şale, A.G., Mikailzade, F.: Structure and magnetic properties of La_{0.60}Sr_{0.33}MnO₃ thin films derived using sol-gel technique. *J. Supercond. Nov. Magn.* **25**, 2767 (2012)
- Han, H., Kim, D., Chu, K., Park, J., Nam, S.Y., Heo, S., et al.: Enhanced switchable ferroelectric photovoltaic effects in hexagonal ferrite thin films via strain engineering. *ACS Appl. Mater. Interfaces* **10**, 1846 (2018)
- Shah, D., Catellani, A., Reddy, H., Kinsey, N., Shalaev, V., Boltasseva, A., Calzolari, A.: Controlling the plasmonic properties of ultra-thin TiN films at the atomic level. *ACS Photonics* **5**, 2816 (2018)
- Fang, Y.Y., Xie, J., Tolle, J., Roucka, R., D'Costa, V.R., Chizmeshya, A.V., Menendez, J., Kouvetakis, J.: Molecular-based synthetic approach to new group iv materials for high efficiency, low-cost solar cells and Si-based optoelectronics. *J. Am. Chem. Soc.* **130**, 16095 (2008)
- Pezzoli, F., Giorgioni, A., Patchett, D., Myronov, M.: Temperature-dependent photoluminescence characteristics of GeSn epitaxial layers. *ACS Photonics* **3**, 2004 (2016)
- Mohanty, B.C., Jo, Y.H., Yeon, D.H., Choi, I.J., Cho, Y.S.: Stress-induced anomalous shift of optical band gap in ZnO: Al thin films. *Appl. Phys. Lett.* **95**, 062103 (2009)
- Shah, D., Catellani, A., Reddy, H., Kinsey, N., Shalaev, V., Boltasseva, A., Calzolari, A. Controlling the plasmonic properties of ultrathin TiN films at the atomic level. *ACS Photonics* **5**, 2816 (2018)
- Massoud, H.Z., Przewlocki, H.M.: Effects of stress annealing in nitrogen on the index of refraction of silicon dioxide layers in metal-oxide-semiconductor devices. *J. Appl. Phys.* **92**, 2202 (2002)
- Della Gaspera, E., Griggs, J., Ahmed, T., Walia, S., Mayes, E. L., Calzolari, A., Catellani, A., Embden, J.V.: Augmented band gap tunability in indium-doped zinc sulfide nanocrystals. *Nanoscale* **11**, 3154 (2019)
- Hadimani, P.L., Ghosh, S.S., Sil, A.: Preparation of Fe doped ZnO thin films and their structural, magnetic, electrical characterization. *Superlatt. Microstruc.* **120**, 198 (2018)
- Tumbul, A., Aslan, F., Demirozu, S., Goktas, A., Kilic, A., Durgun, M., Zarbalı, M.Z.: Solution processed boron doped ZnO thin films: influence of different boron complexes. *Mater. Res. Express* **6**, 035903 (2019)
- Elsheikh, N.Y., Battisha, I.K., Arais, A.A., Shams, M.S.: Effect of increasing Fe-concentrations on ZnO thin film deposited by solgel spin coater. *Egypt. J. Chem.* **65**, 949 (2022)
- Goktas, A., Aslan, F., Mutlu, İ.H.: Effect of preparation technique on the selected characteristics of Zn1-xCoxO nanocrystalline thin films deposited by sol-gel and magnetron sputtering. *J. Alloy. Compd.* **615**, 765 (2014)
- Nkosi, S.S., Kortidis, I., Motaung, D.E., Malgas, G.F., Keartland, J., Sideras-Haddad, E., Forbes, A., Mwakikungac, B.W., Sinha-Ray, S., Kiriakidis, G.: Orientation-dependent low field magnetic anomalies and room-temperature spintronic material – Mn doped ZnO films by aerosol spray pyrolysis. *J. Alloys Comp.* **579**, 485 (2013)
- Mimouni, R., Kamoun, O., Yumak, A., Mhamdi, A., Boubaker, K., Petkova, P., Amlouk, M.: Effect of Mn content on structural, optical, opto-thermal and electrical properties of ZnO:Mn sprayed thin films compounds. *J. Alloys Comp.* **645**, 100 (2015)
- Wang, C., Chen, Z., He, Y., Li, L., Zhang, D.: Structure, morphology and properties of Fe-doped ZnO films prepared by facing target magnetron sputtering system. *Appl. Surf. Sci.* **255**, 6881 (2009)
- Nirmala, M., Anukaliani, A.: Synthesis and characterization of undoped and TM (Co, Mn) doped ZnO nanoparticles. *Mater. Lett.* **65**, 2645 (2011)
- Goktas, A., Aslan, F., Tumbul, A., Gunduz, S.H.: Tuning of structural, optical and dielectric constants by various transition metal doping in ZnO:TM (TM=Mn, Co, Fe) nanostructured thin films: a comparative study. *Ceramics Int.* **43**, 704 (2017)
- Yang, S., Man, B.Y., Liu, M., Chen, C.S., Gao, X.G., Wang, C.C., Hu, B.: Structural, optical and magnetic properties of Zn1-xCox O dilute magnetic semiconductors thin films by pulsed laser deposition. *Phys. B* **405**, 4027 (2010)
- Wang, L.W., Xu, Z., Zhang, F.J., Zhao, S.L., Lu, L.F.: Structural optical and magnetic properties of Mn-doped ZnO films prepared by sputtering. *Int. J. Min. Met. Mater.* **17**, 475 (2010)
- Elanchezhian, J., Bhuvana, K.P., Gopalakrishnan, N., Balasubramanian, T.: Investigation on Mn doped ZnO thin films grown by RF magnetron sputtering. *Mater. Lett.* **66**, 3379 (2008)
- Gopalakrishnan, N., Balakrishnan, L., Brindha, A., Jayalakshmi, G.: Thickness and substrate orientation dependence of ferromagnetism in Mn doped ZnO thin films. *Cryst. Res. Technol.* **47**, 45 (2012)
- Change, Y.Q., Wang, P.W., Tang, R.H., Sun, Q.L., Long, Y.: Synthesis and room temperature ferromagnetism of flower-shaped Mn doped ZnO nanostructures. *J. Mater. Sci. Technol.* **27**, 513 (2017)

35. Sharma, P., Gupta, A., Rao, K. V., Owens, F. J., Sharma, R., Ahuja, R., Gillen, J.M.O., Johansson, B., Gehring, G.A.: Ferromagnetism above room temperature in bulk and transparent thin films of Mn-doped ZnO. *Nat. Mater.* **2**, 673 (2003)
36. Kim, Y.M., Yoon, M., Park, I.W., Park, Y.J., Lyou, J.H.: Synthesis and magnetic properties of Zn_{1-x}Mn_xO films prepared by the sol-gel method. *Solid State Commun.* **129**, 175 (2004)
37. Pradhan, A.K., Zhang, K., Mohanty, S., Dadson, J.B., Hunter, D., Zhang, J., Sellmyer, D.J., Roy, U.N., Cui, Y., Burger, A., Mathews, S., Joseph, B., Sekhar, B.R., Roul, B.K.: High-temperature ferromagnetism in pulsed-laser deposited epitaxial (Zn, Mn)O thin films: effects of substrate temperature. *Appl. Phys. Lett.* **86**, 152511–152512 (2005)
38. Goktas, A., Mutlu, I.H., Yamada, Y., Celik, E.: Influence of pH on the structural optical and magnetic properties of Zn_{1-x}Mn_xO thin films grown by sol-gel method. *J. Alloys Compd.* **553**, 259 (2013)
39. Eriksson, O., Bergqvist, L., Sanyal, B.J.: Electronic structure and magnetism of diluted magnetic semiconductors. *Phys. Condens. Matter.* **16**, 5481 (2004)
40. Venkatesan, M., Fitzgerald, C.B., Coey, J.M.D.: Thin films: unexpected magnetism in a dielectric oxide. *Nature* **430**, 630 (2004)
41. Song, C., Pan, S.N., Liu, X.J., Li, X.W., Zeng, F., Yan, W.S., He, B., Pan, F.: Evidence of structural defect enhanced room-temperature ferromagnetism in Co-doped ZnO. *J. Phys. Condens. Matter.* **19**, 176229 (2007)
42. Cong, C.J., Hong, J.H., Zhang, K.L.: Effect of atmosphere on the magnetic properties of the Co-doped ZnO magnetic semiconductors. *Mater. Chem. Phys.* **113**, 435 (2009)
43. Lawes, G., Risbud, A.S., Ramirez, A.P., Seshadri, R.: Absence of ferromagnetism in Co and Mn substituted polycrystalline ZnO. *Phys. Rev. B* **71**, 045201 (2005)
44. Moreno, M.S., Kasama, T., Dunin-Borkowski, R.E., Cooper, D., Midgley, P.A., Steren, L.B., Duhalde, S., Vignolo, M.F.: Local study of the magnetism of Co-doped ZnO thin films. *J. Phys. D Appl. Phys.* **39**, 1739 (2006)
45. Belghazi, Y., Aouaj, M.A., El Yadari, M., Schmerber, G., Ulhaq-Bouillet, C., Leuvrey, C., Colis, S., Abd-Lefdil, M., Berrada, A., Dinia, A. Elaboration and characterization of Co-doped ZnO thin films deposited by spray pyrolysis technique. *Microelect. J.* **40**, 265 (2009)
46. Polat, İ., Aksu, S., Altunbaş, M., Bacaksız, E.: Microstructural, optical and magnetic properties of cobalt-doped zinc oxysulfide thin films. *Mater. Chem. Phys.* **130**, 800 (2011)
47. Bacaksız, E., Aksu, S., Basol, B.M., Altunbaş, M., Parlak, M., Yanmaz, E.: Structural, optical and magnetic properties of Zn_{1-x}CoxO thin films prepared by spray pyrolysis. *Thin Solid Films* **516**, 7899 (2008)

Publisher's Note Springer Nature remains neutral with regard to jurisdictional claims in published maps and institutional affiliations.

Springer Nature or its licensor (e.g. a society or other partner) holds exclusive rights to this article under a publishing agreement with the author(s) or other rightsholder(s); author self-archiving of the accepted manuscript version of this article is solely governed by the terms of such publishing agreement and applicable law.